Hindawi
Advances in Meteorology
Volume 2023, Article ID 2730839, 15 pages
https://doi.org/10.1155/2023/2730839

Research Article

Modelling the Impacts of the Changing Climate on Streamflow in Didesa Catchment, Abay Basin, Ethiopia

Amsalu Gudeta Awetu[1] and Tadesse Tujuba Kenea[2]

[1]*Faculty of Water Resources and Irrigation Engineering, Water Technology Institute, Arba Minch University, P.O. Box 21, Arba Minch, Ethiopia*
[2]*Faculty of Meteorology and Hydrology, Water Technology Institute, Arba Minch University, P.O. Box 21, Arba Minch, Ethiopia*

Correspondence should be addressed to Tadesse Tujuba Kenea; tade2j@gmail.com

Received 7 November 2022; Revised 28 June 2023; Accepted 4 July 2023; Published 12 July 2023

Academic Editor: Anzhen Qin

The Didesa catchment, which is the second largest subbasin of the Abay basin, significantly contributes to the Blue Nile's outflow. Understanding the dynamics of water availability under the changing climate in such a basin assists in the proper planning of land use and other development activities. This study presents changes in climatic elements such as rainfall, temperature, and evapotranspiration using observation data and regional climate models (RCMs) under two representative concentration pathways (RCPs) for three future periods. We use a calibrated hydrological model to further assess climate change's effects on streamflow. We select three RCMs and their ensemble's mean by evaluating their performance with respect to observations. We apply the modified Mann–Kendall test to detect trends in each dataset. The result shows that annual mean maximum and minimum temperatures increase in the catchment for the 2021–2040, 2041–2070, and 2071–2100 periods as compared to baseline (1989–2018) under both RCP4.5 and RCP8.5 scenarios. Annual mean maximum temperature and potential evapotranspiration experienced a significant decreasing trend during the year from 1989 to 2018. Furthermore, there was an increasing trend in annual rainfall from 1989 to 2018, which could be related to the cooling of sea surface temperature over the equatorial Pacific. We detect an increasing trend in temperature in both scenarios and all periods; however, no clear trend pattern is found in rainfall. The result from hydrological model simulations reveals that the mean monthly streamflow slightly increases in the winter season while it decreases during the main rainy season. Further study of detailed weather systems, which affect the subbasin's climate, is recommended.

1. Introduction

About half of the global population is experiencing severe water scarcity due to climatic and nonclimatic factors for some part of the year. The hydrological cycle is intensified due to anthropogenic climate change, which is affecting the physical aspects of water security. This has exacerbated water-related vulnerabilities caused by other socioeconomic factors [1]. The recent drying trends since the 1980s match the warming observed across the continent of Africa [2], including Ethiopia [3].

The change in climate is a major challenge that affects the hydrological cycle. Besides, the Intergovernmental Panel on Climate Change (IPCC) assessment report shows that the global average temperature would rise with an increasing total carbon dioxide concentration. Furthermore, climate change induces changes in tributary flow characteristics and changes in rainfall patterns, affecting the interception process and changing the evapotranspiration process [4, 5].

Developing countries are likely among the most vulnerable to the impacts of the changing climate due to the lack of economic development and institutional capacity [6]. The impacts of climate change have the potential to weaken and even reverse the progress made in improving the socioeconomic well-being of African countries [7].

Ethiopia and other developing nations will be more susceptible to the effects of climate change. A large part of the country is arid and semiarid, making it highly prone to

drought and desertification. Therefore, the country should be concerned about climate change and its effects. According to Wara et al. [8], the change in climate is projected to cause more frequent and intense ENSO events, leading to widespread drought in the area. Hence, assessing vulnerability to climate change impact and preparing adaptation options as a part of the national program are very crucial [9].

Despite the observed drying trends and frequent droughts in recent years in Ethiopia (e.g., [3, 10], and [11]), only a few studies assessed the impact on water availability in watersheds which is caused by climate change. In addition, there has been some inconsistency in the findings of these investigations. For example, Dile et al. [12] and Adem et al. [13] projected an increase in streamflow at the end of the 21st century in the Gilgel Abay catchment, Abay basin. On the contrary, Setegn et al. [14] projected a decrease in the streamflow of the Lake Tana catchment for the same period. The Didesa catchment is a subbasin of the Abay basin having the second largest area and contributing about 10.9% to the outflow of the Blue Nile River. Therefore, a detailed analysis of the impact of climate change using recent climate models and appropriate hydrological models is essential.

Many earlier researchers used different climate models to understand climate change's effects on surface water availability both for the baseline and future periods [15]. The difference in results of the climate change's effects on streamflow for the same basin is due to the choice of the general circulation model (GCM) and downscaling technique, and the selection of the hydrological model [16]. Therefore, the selection of recently developed climate models with appropriate downscaling techniques is vital.

The impact of climate change can vary in different catchments with relatively small areas due to local climate and catchment characteristics. Altered frequency and distribution of rainfall events, with associated consequences, have effects on discharge rates and streamflow characteristics of the river basin [17]. Climate change impact includes changes in the magnitude of runoff, changes in the frequency of floods and droughts, rainfall patterns, extreme weather events, and the amount of surface water availability [18].

This study aims to assess the change in climatic elements such as rainfall, temperature, and potential evapotranspiration and evaluate their impacts on streamflow in current and projected future periods in the Didesa catchment. Therefore, we identify changes and trends from observations and modelling. This study strongly assists in planning land use and other development activities in a way that fits the dynamism of water availability under the changing climate.

2. Materials and Methods

2.1. Study Area. The study is carried out in the Didesa catchment, which is part of the Abay basin and lies between latitudes of 7.7°N and 10°N and longitudes of 35.5°E and 37.3°E. Its catchment area is 17,645.5 km^2, with an average length of 1368.3 km and a width of 1453.1 km. The elevation varies between 852 m and 3041 m above mean sea level (amsl), with both flat and steep slopes (Figure 1). The catchment is characterized by warm, humid tropics, with a long rainy season (locally known as Kiremt) lasting from June to September with an average annual rainfall between 1450 mm and 2050 mm.

The dry season, which is locally called Bega, extends from November to February. The annual maximum and minimum temperatures in the subbasin vary between 21°C to 30°C and 10°C to 20°C, respectively, during the period of 1989–2018. Annual mean rainfall peaks in the months of June to September, which is the main rainy season for the area (Figure 2).

From a hydrogeological point of view, sedimentary rocks are exposed to the land surface due to regional tectonic activity in the Didesa catchment. Alluvial soils and eluvial soils are developed from granitoid, basalt, Mesozoic sandstone, and Paleozoic sediments in the catchment. The yields of the wells in these aquifers range from 0.5 to about 10 l/s [19].

2.2. Data. We obtain daily rainfall and maximum and minimum temperature data from the Ethiopian Meteorology Institute (EMI). Flow, digital elevation model (DEM), land use land cover, and soil data are acquired from the Ministry of Water and Energy, Ethiopia. We get RCMs output for historical and projected future climate under two different RCPs (RCP4.5 and RCP8.5) from the Coordinated Regional Climate Downscaling Experiment (CORDEX) project (https://esgf-node.llnl.gov/search/esgf-llnl/). This study uses Climate Limited-Area Modelling Community (CCML-4), Regional Atmospheric Climate Model (RACMO22T), Max Planck Institute Regional Model (REMO2009), and their Ensemble's mean. The periods are divided into historical (1989–2018) and three projected future periods: near-term (2021–2040), mid-term (2041–2070), and long-term (2071–2100).

2.3. Methods. We use the physically based soil and water assessment tool (SWAT) model [20] to determine climate change's effects on streamflow due to its simple and powerful tools for modelling [21]. We employ measured flow from 2000 to 2013 years for model calibration and validation. The soil, land use/land cover, DEM, and climate data are inputs to the model for simulating catchment surface runoff.

During the data preparation phase, we convert the point rainfall to its corresponding area estimate using the Thiessen polygon method [22]:

$$R = \sum_{i=1}^{n} \frac{R_i \times A_i}{A}, \tag{1}$$

where R_i is the rainfall measure at a station i, A_i is the area of subcatchment covered by a station i, and A is the total area of the catchment.

We compute the potential evapotranspiration using the Hargreaves method as in Droogers and Allen [23] and Byakatonda et al. [24]:

$$ET_0 = 0.000938 R_a \left(T_{\text{mean}} + 17.8\right) \sqrt{T_{\max} - T_{\min}}, \tag{2}$$

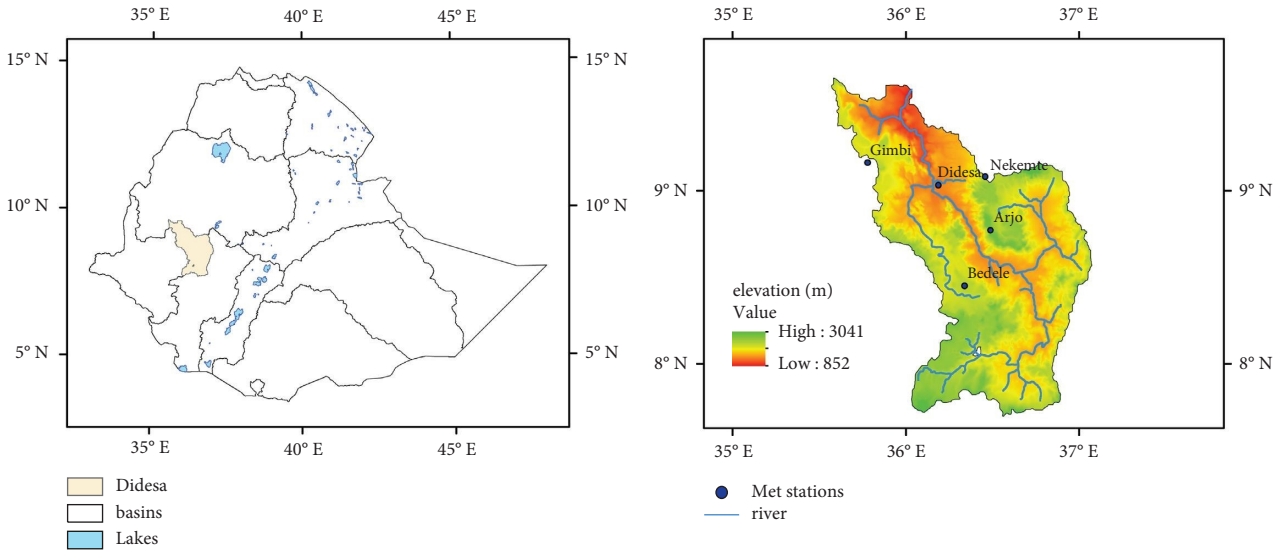

FIGURE 1: Didesa catchment: (a) its location with respect to Ethiopian river basins and (b) its elevation and meteorological stations distribution.

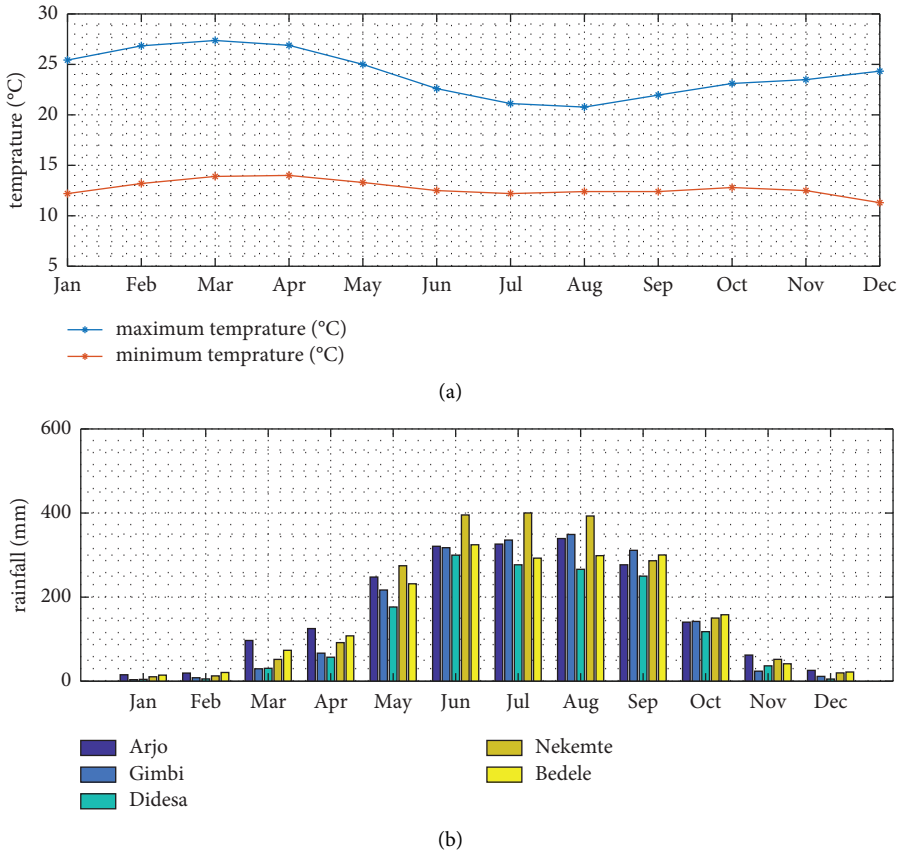

FIGURE 2: Climate of the Didesa catchment averaged over the period of 1989–2018: (a) temperature climatology and (b) precipitation climatology for the catchment.

where T_{mean} is the daily mean temperature in °C, T_{max} is the daily maximum temperature in °C, T_{min} is the daily minimum temperature in °C, and R_a is the extraterrestrial radiation (in MJ·m^{-2}·day^{-1}). The mean extraterrestrial radiation (R_a) is estimated from the latitude of the station and the month of the year.

Outputs of regional climate models cannot be directly used for impact assessment as the computed variables may differ systematically from the observed ones [25, 26]. Therefore, we apply bias corrections to compensate for any tendency to overestimate or underestimate the downscaled variables. We use power transformation for rainfall bias correction. It is a nonlinear method, which corrects both the mean and variance of rainfall as explained by Terink et al. [27]. We apply the correction method by comparing the daily observed rainfall at each station with the outputs of RCMs. On the other hand, we apply the variance scaling method to correct biases in temperature [28]. The temperatures are bias corrected by the following equation:

$$T_{\text{corr}} = \overline{T}_{\text{obs}} + \frac{\sigma T_{\text{obs}}}{\sigma T_{\text{rcm}}} \left(T_{\text{rcm}} - \overline{T}_{\text{rcm}}\right), \tag{3}$$

where T_{corr} is the bias-corrected temperature; T_{rcm} is the raw temperature from the RCM model; σT_{obs} and σT_{rcm} are the standard deviations of the observed and the RCM model output temperature while $\overline{T}_{\text{obs}}$ and $\overline{T}_{\text{rcm}}$ are the mean temperatures from the observation and the RCM model, respectively.

We evaluate the RCMs using statistical measures such as bias, root mean squared error (RMSE), and coefficient of variation (CV) and their performance to reproduce the annual cycle of rainfall. The equations of these statistical measures are as follows:

$$Bias = \frac{\sum (M)}{\sum (O)}, \tag{4}$$

where M is the model output, O is observation, and N is number of observation.

A value of 1 is the perfect score. A bias value above/below 1 indicates an aggregate model overestimation/underestimation.

$$RMSE = \sqrt{\frac{\sum (O - M)^2}{N}}, \tag{5}$$

$$CV = \frac{\sigma}{\overline{x}} \times 100\%, \tag{6}$$

where σ is the standard deviation and $\overline{x}$ is the mean of the data under consideration.

We employ the modified nonparametric MK trend test to assess trends in different climatic elements. Studies widely use the MK trend test as it does not require the data to be normally distributed [24]. It requires the time series data to be serially independent [29]. Thus, an autocorrelation test is applied to determine the presence of serial correlations in the time series data. To remove autocorrelation from time series data, trend-free prewhitening (TFPW), the most used technique, was used [29, 30]. The computation of MK statistics uses S statistics. The S statistics is given by the following equation:

$$S = \sum_{i=1}^{n-1} \sum_{j=i+1}^{n} sgn\left(X_j - X_i\right), \tag{7}$$

where X_j and X_i are the time series observations in chronological order, and n is the length of the time series, while sgn is given by the following equation:

$$sgn\left(X_j - X_i\right) = \begin{cases} +1 & if \left(X_j - X_i\right) > 0, \\ 0 & if \left(X_j - X_i\right) = 0, \\ -1 & if \left(X_j - X_i\right) < 0. \end{cases} \tag{8}$$

Positive values of the S statistic indicate an increasing trend while negative values indicate a decreasing trend [24]. The variance (V) of **S** is calculated as follows:

$$V(S) = \frac{1}{18}\left[n(n-1)(2n+5) - \sum_{p=1}^{q} t_p\left(t_p - 1\right)\left(2t_p + 5\right)\right], \tag{9}$$

where n is the length of time series, t_p is the number of ties for p^{th} value, and q is the number of tied values [29]. The standardized test statistics **Z** is then computed using **S** and the variance $V(S)$ as given by equation 19:

$$Z = \begin{cases} \dfrac{S-1}{\sqrt{V(S)}} & if\ S > 0, \\ 0 & if\ S = 0, \\ \dfrac{S+1}{\sqrt{V(S)}} & if\ S < 0. \end{cases} \tag{10}$$

Positive Z values designate an increasing trend in the time series whereas negative Z values indicate a negative trend. Given a confidence level, α a statistically significant trend is said to be existing in a time series data if $|Z| > Z_{1-(\alpha/2)}$. The level of significance employed in this study is $\alpha = 0.05$, and from the standard normal table, the value of $Z_{1-(\alpha/2)}$ at the level of significance $\alpha = 0.05$ is 1.96.

This study classifies the catchment into multiple subwatersheds, which are further subdivided into a hydrologic response unit (HRU) with unique characteristics of land use management, topography, and soil (Figure 3). SWAT simulates hydrological parameters at each HRU using the water balance equation:

$$SW_t = SW_o + \sum_{i=1}^{t} \left(R_{\text{day}} - Q_{\text{surf}} - E_a - W_{\text{seep}} - Q_{gw}\right), \tag{11}$$

where SW_o and SW_t denote the initial and final volumes of water in the soil (mm); R_{day}, Q_{surf}, E_a, W_{seep}, and Q_{gw} are the rainfall amounts, surface runoff amount, evapotranspiration amount, infiltration amount, and return flow amount on day i (mm) in respective order; and t is the time in days. By using the Soil Conservation Service-Curve Number (SCS CN) method [31], SWAT can be used to evaluate the relative impact of climate change at the catchment level [32, 33].

The subbasin runoff is routed to obtain the total runoff for the entire basin. Surface runoff is computed by using SCS CN as in the following equation:

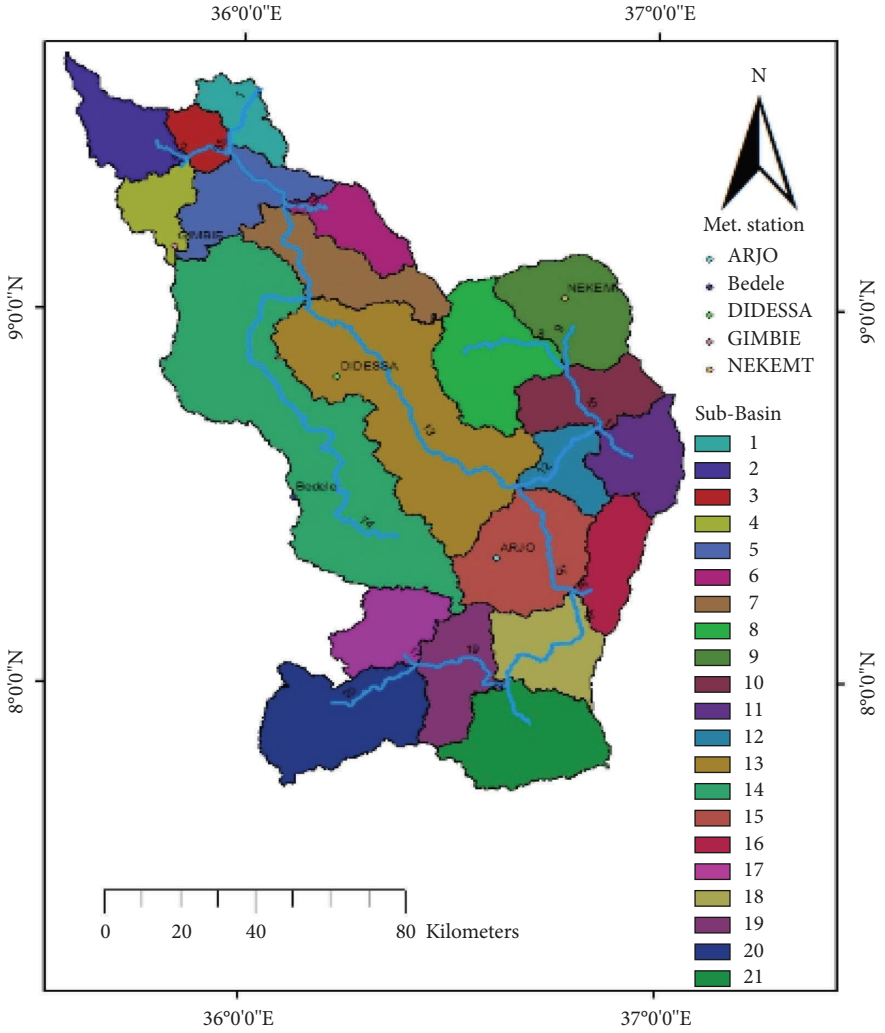

Figure 3: Subbasin delineation of the Didesa catchment.

$$Q_{\text{surf}} = \frac{\left(R_{day} - 0.2S\right)^2}{\left(R_{day} + 0.8S\right)}, \tag{12}$$

where Q_{surf} is the daily surface runoff (mm), R_{day} is the rainfall depth for the day (mm), and S is the retention parameter (mm). The retention parameter (S) is calculated as in the following equation:

$$S = 25.4\left(\frac{1000}{CN} - 10\right), \tag{13}$$

where S is drainable volume of soil water per unit area of saturated thickness (mm/day), and CN is curve number.

Water yield is the aggregate sum of water leaving the HRU and entering the main channel during the time step [34]. The total water yield is computed as follows:

$$W_{yld} = Q_{\text{surf}} + Q_{gw} + Q_{lat} - T_{\text{loss}}, \tag{14}$$

where W_{yld} is the measure of water yield (mm), Q_{surf} is the surface runoff (mm), Q_{lat} is the lateral flow contribution to streamflow (mm), Q_{gw} is the groundwater contribution to streamflow (mm), and T_{loss} is the transmission losses (mm) from tributary in the HRU by means of transmission through the bed.

After having all the necessary spatiotemporal data required by the SWAT, we quantify model sensitivity to parameter changes, as it is a vital step before model calibration. Hydrological parameters are selected for sensitivity analysis for the simulation of streamflow with default lower and upper bound parameter values. In addition to hydrological parameters, the observed monthly flow values are used.

The SWAT model is calibrated and validated with the streamflow observed at the gauging station during the baseline period. We use two-thirds of the data for calibration (2000–2009) and one-third for validation (2010–2013). During the calibration process, the model parameters are subjected to adjustments to obtain model results that correspond better to the measured data sets. Calibration and validation stages are done under SWAT-CUP software support.

We evaluate the model performance using the coefficient of determination (R^2), the Nash–Sutcliffe efficiency (NSE), and the percent bias (PBIAS), which are time series-based metrics during the calibration and validation periods.

$$R^2 = \frac{\left[\sum_{i=1}^{n}\left(Q_{obs} - \overline{Q_{obs}}\right)\left(Q_{sim} - \overline{Q_{sim}}\right)\right]^2}{\sum_{i=n}^{n}\left(Q_{obs} - \overline{Q_{obs}}\right)^2 \sum_{i=n}^{n}\left(Q_{sim} - \overline{Q_{sim}}\right)^2},$$

$$NSE = 1 - \frac{\sum_{i=1}^{n}\left(Q_{obs} - Q_{sim}\right)^2}{\sum_{i=1}^{n}\left(Q_{obs} - \overline{Q_{obs}}\right)^2}, \quad (15)$$

$$PBIAS = \frac{\sum_{i=1}^{n}\left(Q_{obs} - Q_{sim}\right)}{\sum_{i=1}^{n} Q_{obs}} \times 100\%,$$

where Q_{obs} and Q_{sim} represent observation and simulated discharge, respectively,

3. Results and Discussion

3.1. Evaluation of Climate Model Performance. We present the evaluation results of the climate models' outputs with respect to the observed data in Table 1 and Figure 4. All RCMs reasonably predicted the monthly rainfall distribution patterns with gauged rainfall in the catchment with only a slight underestimation of the observation (Figure 4). We also use the models' ability to reproduce the long-term mean annual rainfall (annual RF) of the catchment for the best model selection. The observed mean annual rainfall has been 1977.7 mm, while it is 1775.1 mm, 1794.9 mm, 1807.4 mm, and 1852.2 mm for the REMO2009, RACMO22T, the ensemble's mean, and CCML-4, respectively (Table 1). The comparison shows good agreement with a slight underestimation. The accuracy of the models is not the same in reproducing the rainfall, with CCML-4 performing best (BIAS = −6.3%) while REMO2009 performs the worst (BIAS = −10.2%). The result indicates that the degree of rainfall variability is almost similar in all models; CCML-4 model (CV = 10.8%), RACMO22T model (CV = 11.2%), and REMO2009 model (CV = 13.0%). As there are some differences between model output and observation, the biases should be corrected before applying for impact assessment. These climate models were reported to perform well in the wide area of East Africa in a previous study [35].

3.2. Trends in Observed Data. In the Mann–Kendall trend test, when $P < \alpha$ ($\alpha = 0.05$ in this study), the null hypothesis (H_o) is rejected; this indicates the existence of a trend in the data under consideration. However, when $P > \alpha$, the null hypothesis is accepted, which shows that the trend is insignificant. Sen's slope is employed to compute the magnitude of the trend, where positive and negative values indicate increasing and decreasing trends, respectively. The trends are significant when they are associated with P values less than 0.05.

The trend analysis for the annual total rainfall amount indicates an increasing value of 7.3 mm per year from 1989 to 2018 (Figure 5(c)). The MK test statistics (S) indicates that there is a nonsignificant increasing trend in rainfall at a significance level of 0.05 with a P value of 0.54 (Figure 5(c)). The increasing trend could be related to the cooling of sea surface temperature over the equatorial Pacific, which is reported to have a positive impact in increasing rainfall amount over west Ethiopia [36, 37]. Diro et al. [36] found that a warm (cold) sea surface temperature anomaly over the equatorial Pacific is associated with rainfall deficit (excess) in western Ethiopia during the main rainy season. Similarly, Dufera et al. [37] indicated that there is a negative correlation between sea surface temperature over the equatorial Pacific and drought magnitudes in western Ethiopia during the same season. However, further investigation of the weather systems is required to fully address the cause of the current wetting trend in the subbasin.

Mean annual maximum temperature shows a significant decreasing trend with a negative Sen's slope value and a P value of 0.02 at a significance level of 0.05 (Figure 5(a)) over the period from 1989 to 2018. In addition, the minimum temperature shows a nonsignificant decreasing trend over the same period (Figure 5(b)). The statistics for the trend of minimum temperature is −0.19, 0.30, and −0.02 for Kendall's tau, P value, and Sen's slope, respectively. The weather systems affecting the area's climate should be further investigated in future studies.

3.3. Trends in Projected Climate. As indicated in Table 2, the trend in annual rainfall is not clear. The selected models do not consistently show similar trend patterns. Furthermore, the identified trends are insignificant in both scenarios and all periods except RACMO22T under RCP8.5 in the near-term period. The RACMO22T shows an increasing significant trend under the mentioned scenario and period.

The mean monthly changes in maximum temperature for the future period are shown in Table 3. The trend in maximum temperature shows an increasing trend in both scenarios and all future periods. The mean minimum temperature also shows similar trend patterns (Table 4). An increasing rate of evapotranspiration, a decreasing availability of water resources, and an increasing water demand are expected when the temperature is increasing [38].

3.4. Future Climate Change Patterns. The projected climate can be used as input for process-based hydrologic models to assess the impact of climate change on streamflow. We compute the projected change in temperature, rainfall, and potential evapotranspiration under RCP4.5 and RCP8.5 scenarios in three different future times. In the near-term period, the projected change of rainfall from CCLM-4 and REMO2009 indicates a decrease in the amount for the months from February to December under the RCP4.5 scenario (Figure 6). However, it is not consistent under RCP 8.5.

The projected change of mean monthly maximum temperature is 0.53°C (2021–2040), 1.9°C (2041–2070), and 2.6°C (2071–2100) for RCP4.5, and it is 1.61°C (2021–2040), 1.8°C (2041–2070), and 2°C (2071–2100) for RCP8.5. The mean minimum temperature change per annum over the catchment for the short-term, mid-term, and long-term periods is 0.93°C, 1.8°C, and 2°C, respectively, under the RCP4.5 whereas it is 1.05°C, 1.5°C, and 2.4°C under RCP8.5. The seasonal mean maximum temperature changes are 0.76°C, 1.48°C, and 0.53°C for Bega, Belg, and Kiremt seasons, respectively.

Table 1: Climate models' performance evaluation.

	Observed	CCML-4	RACMO22T	REMO2009	Ensemble's mean
Annual RF (mm)	1977.7	1852.2	1794.9	1775.1	1807.4
Bias (%)	...	−6.3	−9.2	−10.2	−8.6
RMSE (mm/yr)	...	33.5	48.9	54.2	45.5
Standard deviation	598.9	199.5	200.4	231.4	210.5
CV (%)	30.3	10.8	11.2	13.0	11.6

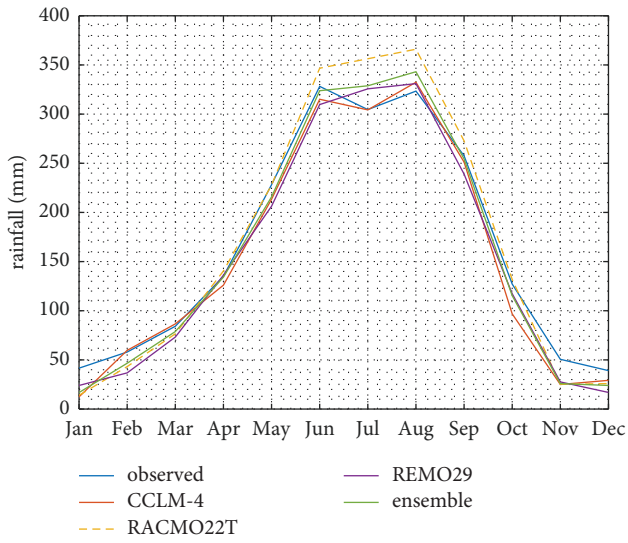

Figure 4: Comparison of mean annual cycle rainfall between models and observation.

The mean change of potential evapotranspiration is mostly positive ranging from 5 to 80 percent in both scenarios and all time periods except some cases during the months of January to May, where the change in potential temperature reaches up to 40 percent (Figure 7). This could be related to the increase in temperature.

3.5. Sensitivity Parameters Analysis. In the analysis, we identify the sensitive parameters of the streamflow. We select parameters for sensitivity analysis to simulate streamflow with default lower and upper bound parameter values as in [39]. The parameters are ranked according to the magnitude of P value and the corresponding t-stat (Table 5). For the global sensitivity analysis, curve number (CN2), base flow alpha factor (ALPHA_BF), groundwater delay time (GW_DELAY), threshold depth of water in the shallow aquifer required for return flow to occur (GWQMN.gw), groundwater re-evaporation coefficient (GW-REVAP.gw), saturated hydraulic conductivity (SOIL_K), soil evaporation compensation factor (ESCO), depth from the soil surface to the bottom of layer (SOIL_Z), deep aquifer percolation fraction (RCHRG_DP), initial depth water in the aquifer (SHALLST_N), manning roughness value for the main channel (CH_N2), channel effective hydraulic conductivity (CH_K2), threshold depth of water in the shallow aquifer for "revap" to occur (REVAPMN.gH), and maximum canopy storage (CANMX) are highly sensitive parameters and ranked from 1 up to 15, respectively. Therefore, curve number (CV), base flow alpha factor (ALPHA_BF), and GW_DELAY are the most sensitive parameters. The t-stat provides a measure of the sensitivity parameters (large absolute values are more sensitive), whereas the P value indicates the significance of the sensitivity. The P value closer to zero means the parameters have more significance.

3.6. Calibration. The parameter ranges are modified automatically based on the correlation between the simulated and observed streamflow while ensuring sufficient parameter space as well as fast convergence. After automatically calibrating, the final results of the calibration are obtained by multiplying, adding, or subtracting the default values by a necessary factor guided by a manual calibration helper. The values of the parameters are varied iteratively within the allowable range until the simulated flow matches the observed streamflow. Figure 8 compares the observed and simulated flow during calibration. At the end of the iteration, the model performance efficiency results in R^2, NSE, and PBIAS values of 0.74, 0.71, and 14.5, respectively.

3.7. Validation. After calibrating and getting acceptable values of R^2, NSE, and PBIAS, validation of the simulated streamflow without further adjustment of the calibrated parameters is performed. The results of the validation show good agreement between the simulated and measured monthly flow with the R^2 value of 0.70, NSE value of 0.67, and PBIAS value of −4.0. The monthly validated result of streamflow is presented in Figure 9.

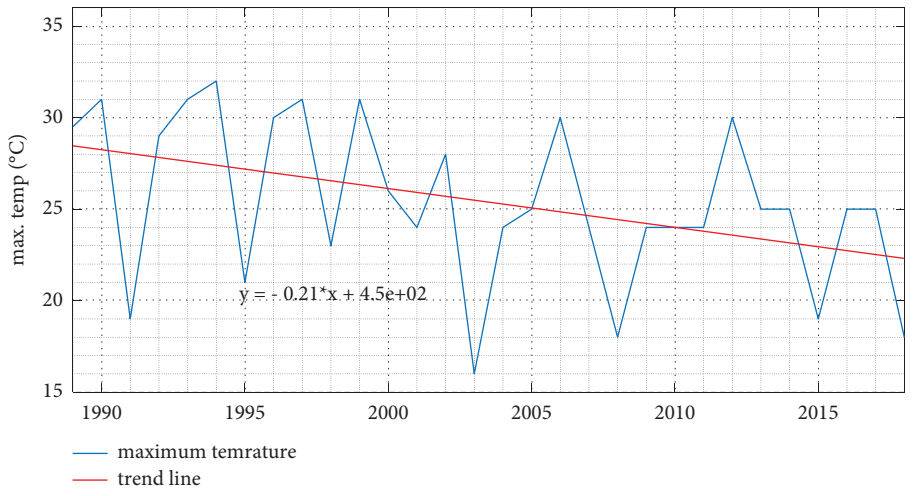

(a)

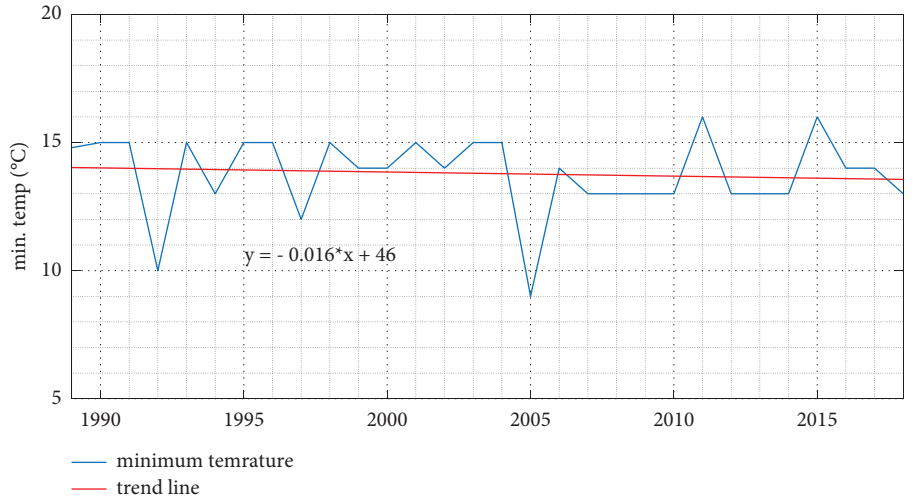

(b)

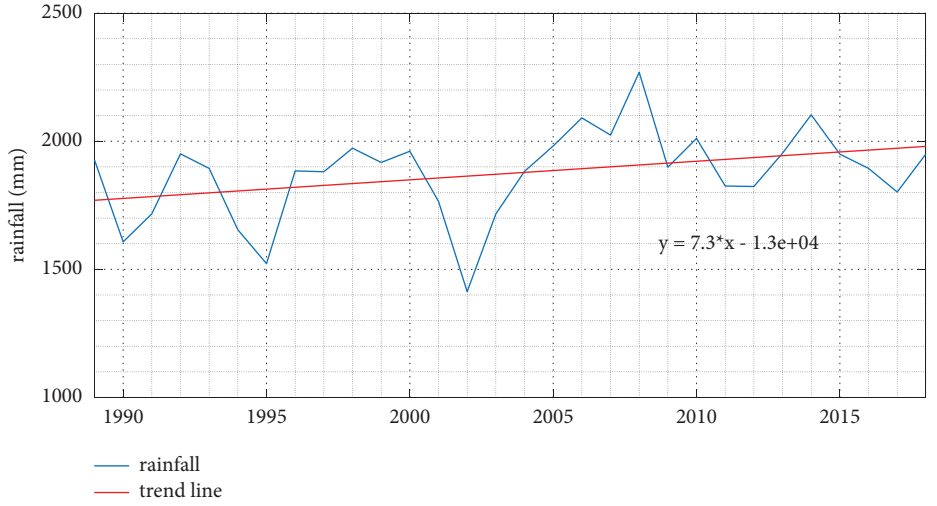

(c)

Figure 5: Trends in observed data of all stations in the Didesa catchment (1989–2018): (a) maximum temperature, (b) minimum temperature, and (c) rainfall. Temperatures are presented as annual mean maximum temperature and annual mean minimum temperature while rainfall is presented as annual total rainfall.

Table 2: Mann–Kendall trend test for annual rainfall. S is Sen's slope, P value (two-tailed) test statistics. A significance level, $\alpha = 0.05$, is used. The (−) sign represents a decreasing trend.

Models	RCP 4.5						RCP 8.5					
	Near-term		Mid-term		Long-term		Near-term		Mid-term		Long-term	
	P	S	P	S	P	S	P	S	P	S	P	S
CCLM-4	0.5	−3.1	1.0	0.1	0.2	−5.6	0.6	−2.7	0.1	−9.0	0.2	−5.3
RACMO22T	0.1	8.7	0.4	−4.2	0.5	6.5	0.01	10.9	0.1	9.7	0.2	8.7
REMO2009	0.1	5.7	0.4	4.1	0.6	4.5	0.9	0.2	0.5	4.5	0.1	9.5
Ensembles	0.3	2.4	0.7	−1.0	0.6	4.0	0.3	2.4	0.1	3.0	0.8	5.9

Table 3: MK trend test for maximum temperature (°C) per year for near-term, mid-term, and long-term projections under both RCP scenarios in the Didesa catchment.

Models			CCLM-4	RACMO22T	REMO2009	Ensembles
RCP 4.5	Near-term	P value	0.01	0.0001	0.0002	0.0001
		S-slope	0.03	0.05	0.05	0.05
	Mid-term	P value	0.002	0.0002	0.01	0.0001
		S-slope	0.04	0.07	0.05	0.05
	Long-term	P value	0.51	0.02	0.40	0.01
		S-slope	0.01	0.03	0.01	0.05
RCP 8.5	Near-term	P value	0.002	0.0001	0.002	0.0001
		S-slope	0.05	0.07	0.04	0.05
	Mid-term	P value	0.0001	0.0001	0.0001	0.0001
		S-slope	0.11	0.10	0.09	0.10
	Long-term	P value	0.0001	0.0001	0.0001	0.0001
		S-slope	0.12	0.11	0.10	0.33

Table 4: MK trend test for minimum temperature (°C) per year for near-term, mid-term, and long-term projections under both RCP scenarios in the Didesa catchment.

Models			*CCLM-4*	*RCMO22T*	*REMO2009*	*Ensembles*
RCP 4.5	Short term	P value	0.0001	0.001	0.001	0.0001
		S-slope	0.03	0.03	0.02	0.02
	Mid-term	P value	0.002	0.0002	0.01	0.0001
		S-slope	0.04	0.07	0.05	0.02
	Long-term	P value	0.72	0.64	0.25	0.30
		S-slope	0.00	0.00	0.01	0.02
RCP 8.5	Short-term	P value	0.001	0.01	0.001	0.0001
		S-slope	0.03	0.02	0.03	0.02
	Mid-term	P value	0.0001	0.0001	0.0001	0.0001
		S-slope	0.11	0.10	0.09	0.02
	Long-term	P value	0.0001	0.0001	0.0001	0.0001
		S-slope	0.05	0.05	0.04	0.13

The model performance result shows a good correlation between the measured and simulated streamflow. Moriasi et al. [40] recommend that model performance can be considered satisfactory for flow simulations if monthly $R^2 > 0.60$, NSE >0.50, and PBIAS ≤ ±15% for watershed-scale models. The performance of the model is presented in Table 6.

3.8. Streamflow under Current Climate. Figure 10 shows the monthly, seasonal, and annual mean streamflow (2000–2013). August and September are months with high rainfall and show peak streamflow with values of 299 m^3/s and 306 m^3/s, respectively (Figure 10(a)). Summer is the longest rainy season in the catchment with a maximum mean seasonal streamflow rate of 204 m^3/s followed by the winter and spring (Figure 10(b)).

3.9. Climate Change Effects on Water Balance Components. The mean monthly rainfall and evapotranspiration in the Didesa catchment during the base period are 156 mm and 113 mm, respectively (Figure 11). The surface runoff amount, lateral flow, groundwater contribution, and transmission loss are about 60 mm, 10 mm, 45 mm, and 7 mm, respectively, for the catchment resulting in a total water yield of 108 mm.

Under a short-term period, the change in average annual components of water balance including rainfall, groundwater flow, and potential evapotranspiration

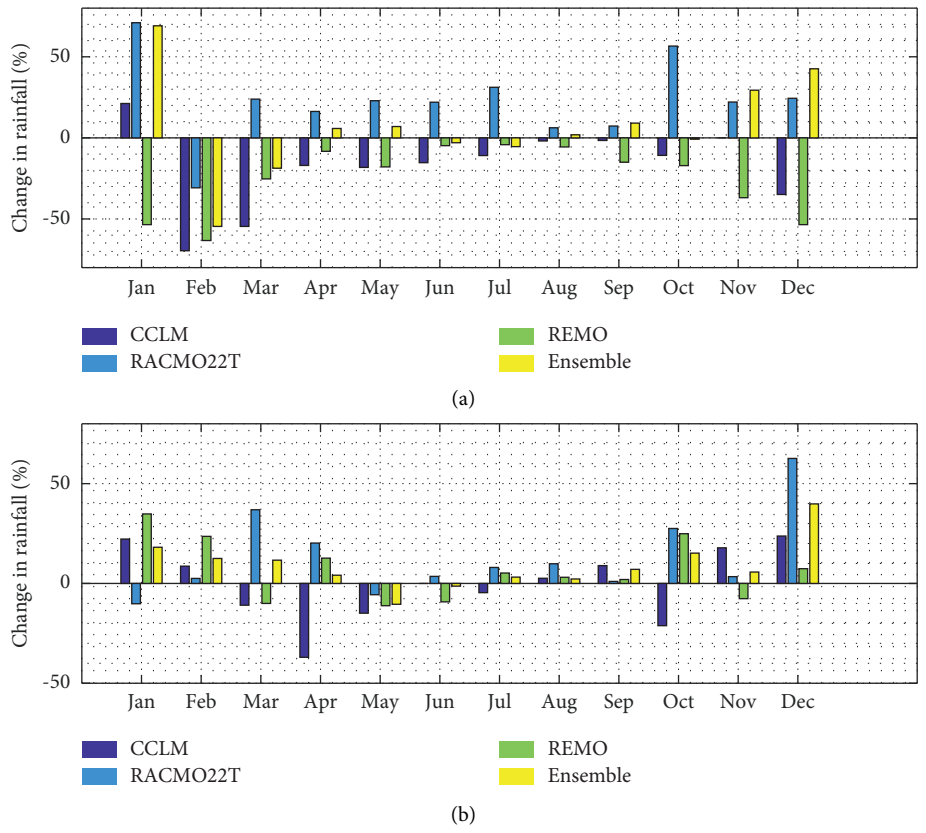

Figure 6: Projected change of average monthly rainfall distribution for near-term (2021–2040) under (a) RCP4.5 and (b) RCP8.5.

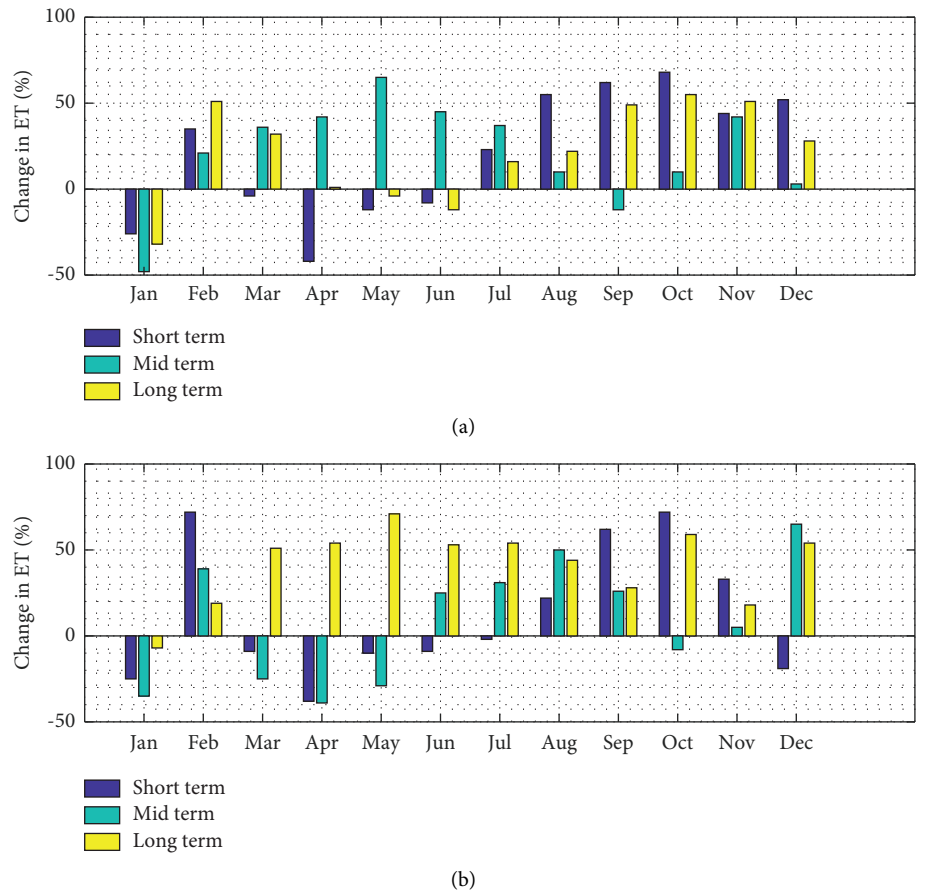

Figure 7: Projected change of mean monthly potential evapotranspiration for short-term (2021–2040), mid-term (2041–2070), and long-term (2071–2100) under (a) RCP4.5 and (b) RCP8.5.

Table 5: The maximum and minimum ranges of the parameter values and their fitted values obtained during the calibration and validation periods.

No.	Parameter name	Fitted value	Min_value	Max_value	*t*-stat	*P* value
1	R__CN2.mgt	41.5	350.0	98.0	0.3	0.05
2	V__ALPHA_BF.gw	0.4	0.0	1.0	−0.4	0.47
3	V__GW_DELAY.gw	23.6	0.0	500.0	−0.6	0.60
4	V__GWQMN.gw	1803.8	0.0	5000.0	0.9	0.12
5	V__GW_REVAP.gw	0.1	0.0	0.2	0.9	0.71
6	R__SOL_K.s	0.4	−0.5	0.5	−1.8	0.28
7	R__ESCO.bsn	0.5	0.0	1.0	1.0	0.62
8	R__SOL_Z.s	0.2	−0.5	0.5	1.2	0.75
9	R__RCHRG_DP.gw	0.4	0.0	1.0	1.8	0.56
10	V__SHALLST_N	1.4	0.0	10.0	−2.4	0.35
11	R__CH_N2.rte	0.3	0.0	1.0	2.5	0.11
12	R__CH_K2.rte	32.4	0.0	150.0	2.7	0.25
13	V__REVAPMN.gw	448.8	0.0	500.0	2.8	0.23
14	R__USLE_P.mgt	1.0	0.0	1.0	−0.7	0.15
15	R__CANMX.hru	7.9	0.0	10.0	−0.5	0.01

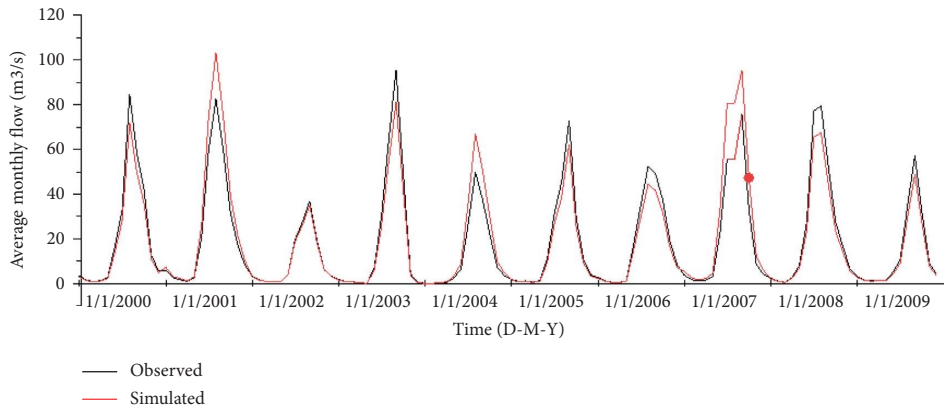

Figure 8: Observed and simulated discharge at the outlet during calibration.

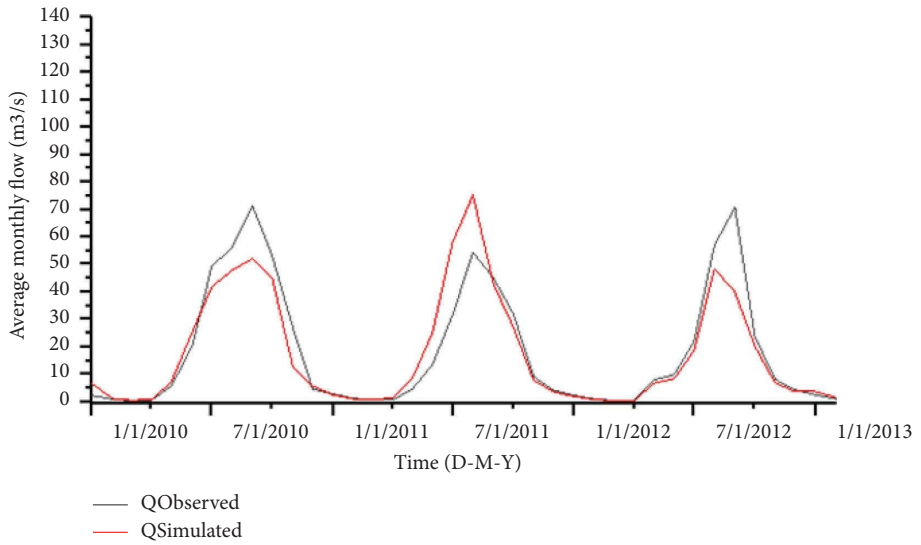

Figure 9: Observed and simulated discharge at the outlet during validation.

Table 6: Comparison of observed and simulated flow during the calibration and validation period.

Period	R^2	NSE	PBIAS
Calibration (2000–2009)	0.74	0.71	14.5
Validation (2010–2013)	0.70	0.67	−4.0

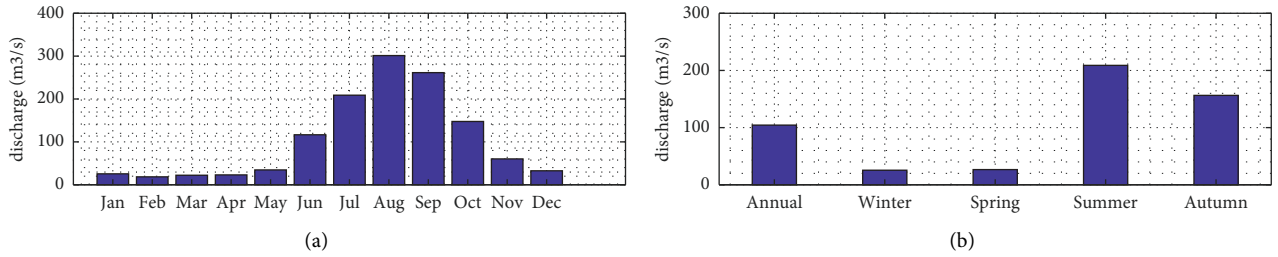

Figure 10: The baseline period average streamflow of (a) monthly and (b) seasonal and annual.

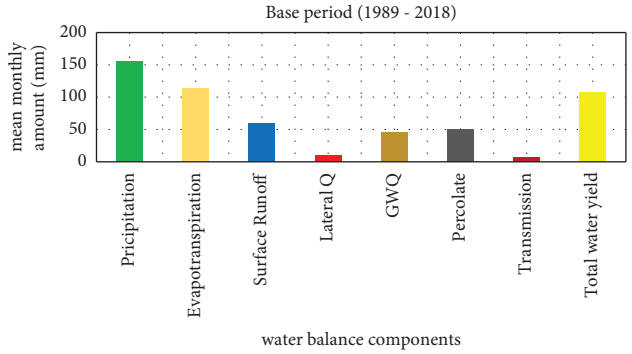

Figure 11: Mean monthly water balance components during 1989–2018.

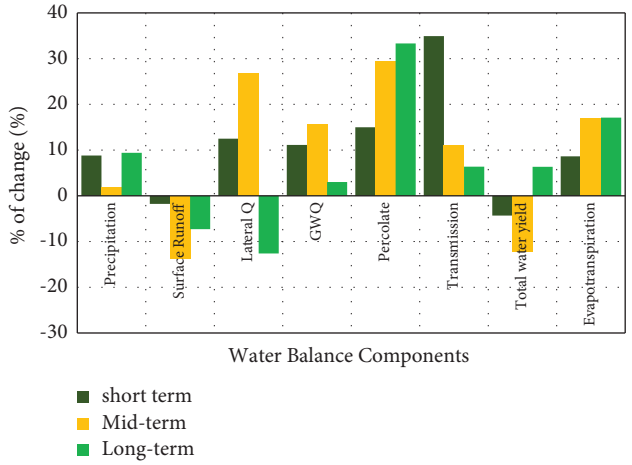

Figure 12: Percentage change of annual mean of water balance components from baseline for short-term, mid-term, and long-term periods.

significantly increases by 8.8%, 11.1%, and 8.6%, respectively. Similarly, the other components such as lateral flow, percolation of water, and transmission loss significantly increase by 12.5%, 15.0%, and 34.9%, respectively, while surface runoff and total water yield decrease by −2% and −4%, respectively (Figure 12). All water balance components increase during the mid-term except surface runoff and total water yield.

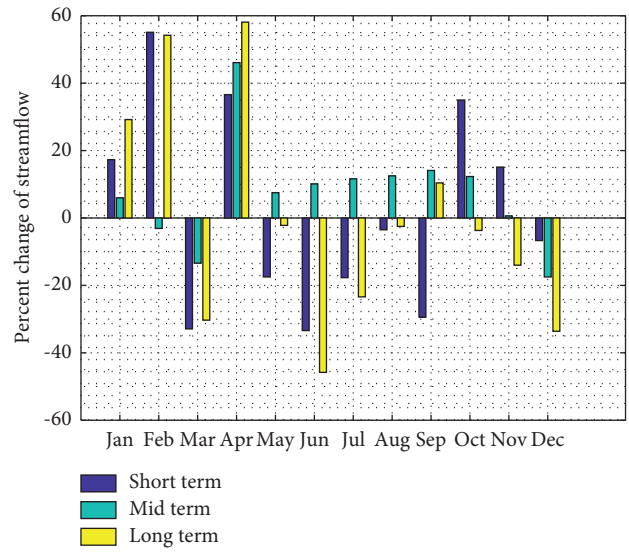

Figure 13: Monthly change in streamflow in the Didesa catchment.

3.10. Climate Change Effects on Mean Streamflow. During the short-term period, the monthly streamflow change in the main river is positive for January, February, April, September, October, and November months, while it is negative for the other months. During the mid-term period, the change in monthly streamflow is positive in all months except the months of February, March, and December. Furthermore, the change in streamflow is positive only in the months of January, February, and April during the long-term period (Figure 13).

The change in streamflow in the Didesa catchment is positive for the annual and winter seasons, while it is negative in other seasons for short-term period as compared to the base period. The change in streamflow is negative during summer and positive during winter in all time periods. This is not a good sign as summer is the main growing season around the catchment (Figure 14). There are

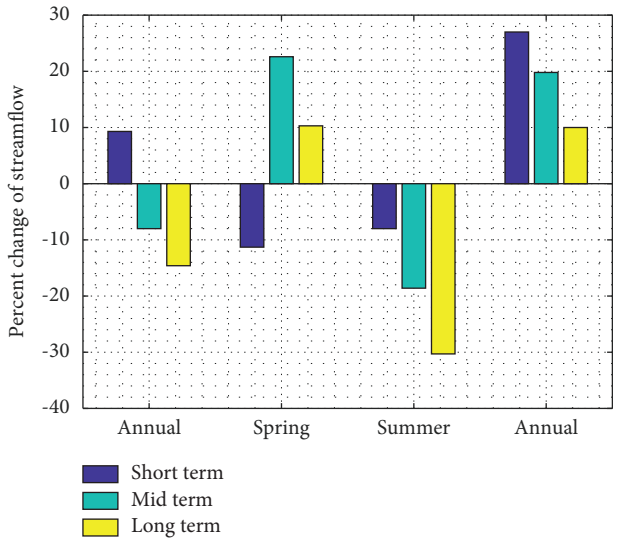

Figure 14: Percentage change in seasonal and annual flow against the baseline period.

irrigation activities that have been practiced in the catchment. Moreover, about 16 and 68 percent of the area are found highly suitable and moderately suitable, respectively, for surface irrigation [41].

4. Conclusions

This study presents the evaluation of the current and future climate change's effects on streamflow in the Didesa catchment for 2021–2040 (near-term), 2041–2070 (mid-term), 2071–2100 (long-term) relative to 1989–2018 using the ensemble's mean of four RCMs output under RCP4.5 and RCP8.5 emission scenarios. The bias correction is performed for future rainfall and temperature before directly using it as input to the hydrological model. The modified Mann–Kendall (MK) trend test for rainfall shows an increasing trend for short-term and mid-term in all periods under both scenarios considered except for RCP4.5 during the mid-term period for RACMO22T and REMO2009 models. However, the CCLM-4 rainfall projection contrastingly shows a decreasing trend in RCP4.5 and RCP8.5 except during mid-term under RCP 4.5, where it shows an increasing trend. The mean change of rainfall is negative for CCLM-4 in the short-term period for the months from February to December, with values ranging from −1.6% to −69.5% under the RCP4.5 scenario. REMO2009 model shows a negative rainfall change in all months under RCP 4.5. The mean minimum temperature change per annum over the catchment for the short-term, mid-term, and long-term periods increases by 0.93°C, 1.8°C, and 2°C, respectively, from the baseline under the RCP4.5 scenario, while it is 1.05°C, 1.5°C, and 2.4°C under RCP8.5 scenario.

July and August are months with mean peak flow in the catchment, which corresponds to periods of high rain. The observed mean annual streamflow shows an increasing trend, with peak flood in 2013 (150.65 m^3/s) and minimum streamflow in 2000 (22.06 m^3/s). This could be related to the increase in rainfall during 1989–2018. The hydrological model performs well with R^2, NSE, and PBIAS values of 0.74, 0.71, and 14.5, respectively, during calibration (2000–2009) and 0.70, 0.67, and −4.0 during validation (2010–2013) periods.

The percent changes in average annual components of water balance are mostly positive, while total water yield shows a decrease during short-term period. Most water balance components increase except surface runoff and total water yield during mid-term period. Under long-term period (2071–2100), the percent changes in average annual water balance component show a significant increase except surface runoff and lateral flow.

In general, a decreasing trend in mean maximum and mean minimum temperature, a decreasing trend in evapotranspiration, and an increasing trend in total annual rainfall are detected during the 1989–2018 period resulting in increasing amount of mean streamflow. While a detailed study of the weather systems of the catchment is recommended, the increase in rainfall could be related to the frequent cooling of sea surface temperature in the equatorial Pacific. On the other hand, an increase in temperature and evapotranspiration with an indefinite pattern of rainfall is expected in future periods. A decrease in streamflow during the main rainy season is expected. Therefore, water resource availability should be included in any planning, and the resources should be used wisely. The result from this study is crucial to plan irrigation projects and to develop drinking water and other activities.

Data Availability

The data supporting the current study are available from the corresponding author upon request.

Conflicts of Interest

The authors declare that there are no conflicts of interest.

Acknowledgments

The authors acknowledge the Ministry of Water and Energy of Ethiopia and the Ethiopian Meteorology Agency for providing the required data free of charge. The first author thanks Arba Minch University for providing him the opportunity to join the master's program in hydrology.

References

[1] H. Pörtner, D. C. Roberts, and H. Adams, *Climate Change 2022: Impacts, Adaptation and Vulnerability*, IPCC, Geneva, Switzerland, 2022.

[2] A. Dai, "Characteristics and trends in various forms of the palmer drought severity index during 1900–2008," *Journal of Geophysical Research*, vol. 116, no. 12, Article ID 12115, 2011.

[3] T. T. Zeleke, F. Giorgi, G. T. Diro, and B. F. Zaitchik, "Trend and periodicity of drought over Ethiopia," *International Journal of Climatology*, vol. 37, no. 13, pp. 4733–4748, 2017.

[4] A. K. Basheer, H. Lu, A. Omer, A. B. Ali, and A. M. Abdelgader, "Impacts of climate change under CMIP5 RCP scenarios on the streamflow in the Dinder River and

ecosystem habitats in Dinder National Park, Sudan," *Hydrology and Earth System Sciences*, vol. 20, no. 4, pp. 1331–1353, 2016.

[5] G. Elias, "Impact of climate change on Lake Chamo water balance, Ethiopia," *International Journal of Water Resources and Environmental Engineering*, vol. 9, no. 4, pp. 86–95, 2017.

[6] L. Bernstein, P. Bosch, O. Canziani, Z. Chen, R. Christ, and K. Riahi, *2007: Climate Change 2007: Synthesis Report*, IPCC, Geneva, Switzerland, 2008.

[7] M. C. Tirado, R. Clarke, L. A. Jaykus, A. McQuatters-Gollop, and J. M. Frank, "Climate change and food safety: a review," *Food Research International*, vol. 43, no. 7, pp. 1745–1765, 2010.

[8] M. W. Wara, A. C. Ravelo, and M. L. Delaney, "Permanent el niño-like conditions during the pliocene warm period," *Science*, vol. 309, no. 5735, pp. 758–761, 2005.

[9] E. G. Beyene and B. Meissner, "Spatio-temporal analyses of correlation between NOAA satellite RFE and weather stations' rainfall record in Ethiopia," *International Journal of Applied Earth Observation and Geoinformation*, vol. 12, pp. S69–S75, 2010.

[10] E. Viste, D. Korecha, and A. Sorteberg, "Recent drought and precipitation tendencies in Ethiopia," *Theoretical and Applied Climatology*, vol. 112, no. 3-4, pp. 535–551, 2013.

[11] T. T. Kenea, J. Kusche, S. Kebede, and A. Güntner, "Forecasting terrestrial water storage for drought management in Ethiopia," *Hydrological Sciences Journal*, vol. 65, no. 13, pp. 2210–2223, 2020.

[12] Y. T. Dile, R. Berndtsson, and S. G. Setegn, "Hydrological response to climate change for gilgel abay river, in the lake tana basin-upper blue Nile basin of Ethiopia," *PLoS One*, vol. 8, no. 10, Article ID 79296, 2013.

[13] A. A. Adem, S. A. Tilahun, E. K. Ayana et al., "Climate change impact on sediment yield in the upper gilgel abay catchment, blue nile basin, Ethiopia," *Landscape Dynamics, Soils and Hydrological Processes in Varied Climates*, pp. 615–644, Springer, Berlin, Germany, 2016.

[14] S. G. Setegn, D. Rayner, A. M. Melesse, B. Dargahi, and R. Srinivasan, "Impact of climate change on the hydroclimatology of Lake Tana basin, Ethiopia," *Water Resources Research*, vol. 47, no. 4, Article ID 04511, 2011.

[15] R. H. Moss, J. A. Edmonds, K. A. Hibbard et al., "The next generation of scenarios for climate change research and assessment," *Nature*, vol. 463, no. 7282, pp. 747–756, 2010.

[16] S. Hagemann, C. Chen, D. B. Clark et al., "Climate change impact on available water resources obtained using multiple global climate and hydrology models," *Earth System Dynamics*, vol. 4, no. 1, pp. 129–144, 2013.

[17] M. A. Osei, L. K. Amekudzi, D. D. Wemegah, K. Preko, E. S. Gyawu, and K. Obiri-Danso, "The impact of climate and land-use changes on the hydrological processes of Owabi catchment from SWAT analysis," *Journal of Hydrology: Regional Studies*, vol. 25, Article ID 100620, 2019.

[18] M. Andargachew and A. Fantahun, "Impact of climate change on hydrological responses of gumara catchment, in the Lake Tana basin-upper blue nile basin of Ethiopia," *International Journal of Water Resources and Environmental Engineering*, vol. 9, no. 1, pp. 8–21, 2017.

[19] S. Kebede, *Groundwater in Ethiopia: Features, Numbers and Opportunities*, Springer Science & Business Media, Berlin, Germany, 2012.

[20] J. G. Arnold, R. Srinivasan, R. S. Muttiah, and J. R. Williams, "Large area hydrologic modeling and assessment part I: model development 1," *Journal of the American Water Resources Association*, vol. 34, no. 1, pp. 73–89, 1998.

[21] D. Mengistu, W. Bewket, A. Dosio, and H. Panitz, "Climate change impacts on water resources in the upper blue nile (Abay) river basin, Ethiopia," *Journal of Hydrology*, vol. 592, no. 2021, Article ID 125614, 2021.

[22] A. H. Thiessen, "Precipitation averages for large areas," *Monthly Weather Review*, vol. 39, no. 7, pp. 1082–1089, 1911.

[23] P. Droogers and R. G. Allen, "Estimating reference evapotranspiration under inaccurate data conditions," *Irrigation and Drainage Systems*, vol. 16, no. 1, pp. 33–45, 2002.

[24] J. Byakatonda, B. P. Parida, D. B. Moalafhi, and P. K. Kenabatho, "Analysis of long term drought severity characteristics and trends across semiarid Botswana using two drought indices," *Atmospheric Research*, vol. 213, pp. 492–508, 2018.

[25] C. Piani, G. P. Weedon, M. Best et al., "Statistical bias correction of global simulated daily precipitation and temperature for the application of hydrological models," *Journal of Hydrology*, vol. 395, no. 3-4, pp. 199–215, 2010.

[26] N. Addor and J. Seibert, "Bias correction for hydrological impact studies–beyond the daily perspective," *Hydrological Processes*, vol. 28, no. 17, pp. 4823–4828, 2014.

[27] W. Terink, R. T. W. L. Hurkmans, P. J. J. F. Torfs, and R. Uijlenhoet, "Evaluation of a bias correction method applied to downscaled precipitation and temperature reanalysis data for the Rhine basin," *Hydrology and Earth System Sciences*, vol. 14, no. 4, pp. 687–703, 2010.

[28] C. Teutschbein and J. Seibert, "Evaluation of bias-correction procedures for adjusting RCM simulations for hydrological impact studies at the catchment scale," in *Proceedings of the American Geophysical Union Fall Meeting 2011*, pp. A23C–A0171, San Francisco, CA, USA, December 2011.

[29] I. Ahmad, D. Tang, T. Wang, M. Wang, and B. Wagan, "Precipitation trends over time using Mann-Kendall and spearman's rho tests in swat river basin, Pakistan," *Advances in Meteorology*, vol. 2015, pp. 1–15, 2015.

[30] S. Yue, P. Pilon, and G. Cavadias, "Power of the Mann–Kendall and Spearman's rho tests for detecting monotonic trends in hydrological series," *Journal of Hydrology*, vol. 259, no. 1-4, pp. 254–271, 2002.

[31] US Soil Conservation Service, *National Engineering Handbook, Section 4: Hydrology*, US Soil Conservation Service, Washington, DC, 1985.

[32] J. G. Arnold and P. M. Allen, "Estimating hydrologic budgets for three Illinois watersheds," *Journal of Hydrology*, vol. 176, no. 1-4, pp. 57–77, 1996.

[33] A. P. Nilawar and M. L. Waikar, "Impacts of climate change on streamflow and sediment concentration under RCP 4.5 and 8.5: a case study in Purna river basin, India," *Science of the Total Environment*, vol. 650, pp. 2685–2696, 2019.

[34] F. Ayivi and M. K. Jha, "Estimation of water balance and water yield in the Reedy Fork-Buffalo Creek Watershed in North Carolina using SWAT," *International Soil and water conservation Research*, vol. 6, no. 3, pp. 203–213, 2018.

[35] G. G. Haile, Q. Tang, S. M. Hosseini-Moghari et al., "Projected impacts of climate change on drought patterns over East Africa," *Earth's Future*, vol. 8, no. 7, Article ID 2020EF001502, 2020.

[36] G. T. Diro, D. I. F. Grimes, and E. Black, "Large scale features affecting Ethiopian rainfall," *African Climate and Climate Change: Physical, Social and Political Perspectives*, vol. 43, pp. 13–50, 2011.

[37] J. A. Dufera, T. A. Yate, and T. T. Kenea, "Spatiotemporal analysis of drought in Oromia regional state of Ethiopia over the period 1989 to 2019," *Natural Hazards*, vol. 117, no. 2, pp. 1569–1609, 2023.

[38] S. Das, P. Datta, D. Sharma, and K. Goswami, "Trends in temperature, precipitation, potential evapotranspiration, and water availability across the teesta river basin under 1.5 and 2° C temperature rise scenarios of CMIP6," *Atmosphere*, vol. 13, no. 6, p. 941, 2022.

[39] A. İrvem and E. S. Ashraf, "Evaluation of streamflow simulation by SWAT model for the seyhan river basin," *Çukurova Tarım ve Gıda Bilimleri Dergisi*, vol. 33, no. 2, pp. 99–110, 2018.

[40] D. N. Moriasi, R. W. Zeckoski, and J. G. Arnold, "Hydrologic and water quality models: key calibration and validation topics," *Transactions of the ASABE*, vol. 58, no. 6, pp. 1609–1618, 2015.

[41] M. B. Moisa, B. B. Merga, and D. O. Gemeda, "Land suitability evaluation for surface irrigation using geographic information system: a case study in Didessa River Sub-Basin, Western Ethiopia," *Sustainable Water Resources Management*, vol. 8, no. 3, p. 82, 2022.